Macroscopic Hierarchical Surface Patterning of Porphyrin Trimers via Self-Assembly and Dewetting

Richard van Hameren, *et al.*

Science **314**, 1433 (2006);
DOI: 10.1126/science.1133004

Science (print ISSN 0036-8075; online ISSN 1095-9203) is published weekly, except the last week in December, by the American Association for the Advancement of Science, 1200 New York Avenue NW, Washington, DC 20005.

terms of fractional resolution but greatly surpasses the latter in signal size. For optical frequency standards, the high resolution presented here has improved studies of systematic errors for the evaluation of clock accuracy. With these narrow resonances, clock instability below 10^{-16} at 100 s is anticipated in the near future. For quantum physics and engineering, this system opens the door to using neutral atoms for experiments in which long coherence times are necessary, motional and internal atomic quantum states must be controlled independently, and many parallel processors are desired.

References and Notes

1. D. Leibfried, R. Blatt, C. Monroe, D. Wineland, *Rev. Mod. Phys.* **75**, 281 (2003).
2. R. J. Rafac *et al.*, *Phys. Rev. Lett.* **85**, 2462 (2000).
3. P. O. Schmidt *et al.*, *Science* **309**, 749 (2005).
4. H. Häffner *et al.*, *Phys. Rev. Lett.* **90**, 143602 (2003).
5. H. Häffner *et al.*, *Nature* **438**, 643 (2005).
6. H. S. Margolis *et al.*, *Science* **306**, 1355 (2004).
7. T. Schneider, E. Peik, C. Tamm, *Phys. Rev. Lett.* **94**, 230801 (2005).
8. P. Dubé *et al.*, *Phys. Rev. Lett.* **95**, 033001 (2005).
9. D. L. Haycock, P. M. Alsing, I. H. Deutsch, J. Grondalski, P. S. Jessen, *Phys. Rev. Lett.* **85**, 3365 (2000).
10. I. Bloch, M. Greiner, in *Advances in Atomic Molecular and Optical Physics* (Academic Press, San Diego, CA, 2005), vol. 52, pp. 1–47.
11. A. T. Black, H. W. Chan, V. Vuletic, *Phys. Rev. Lett.* **91**, 203001 (2003).
12. J. Ye, D. W. Vernooy, H. J. Kimble, *Phys. Rev. Lett.* **83**, 4987 (1999).
13. H. Katori, M. Takamoto, V. G. Pal'chikov, V. D. Ovsiannikov, *Phys. Rev. Lett.* **91**, 173005 (2003).
14. See, for example, *Science* **306**, no. 5700 (2004).
15. T. Zelevinsky *et al.*, *Phys. Rev. Lett.* **96**, 203201 (2006).
16. T. Mukaiyama, H. Katori, T. Ido, Y. Li, M. Kuwata-Gonokami, *Phys. Rev. Lett.* **90**, 113002 (2003).
17. T. H. Loftus, T. Ido, A. D. Ludlow, M. M. Boyd, J. Ye, *Phys. Rev. Lett.* **93**, 073003 (2004).
18. T. H. Loftus, T. Ido, M. M. Boyd, A. D. Ludlow, J. Ye, *Phys. Rev. A* **70**, 063413 (2004).
19. F. Ruschewitz *et al.*, *Phys. Rev. Lett.* **80**, 3173 (1998).
20. U. Sterr *et al.*, *C. R. Phys.* **5**, 845 (2004).
21. T. Ido *et al.*, *Phys. Rev. Lett.* **94**, 153001 (2005).
22. G. Ferrari *et al.*, *Phys. Rev. Lett.* **91**, 243002 (2003).
23. I. Courtillot *et al.*, *Phys. Rev. A* **68**, 030501 (2003).
24. M. Takamoto, F. L. Hong, R. Higashi, H. Katori, *Nature* **435**, 321 (2005).
25. A. D. Ludlow *et al.*, *Phys. Rev. Lett.* **96**, 033003 (2006).
26. R. Le Targat, *Phys. Rev. Lett.* **97**, 130801 (2006).
27. R. Santra, E. Arimondo, T. Ido, C. H. Greene, J. Ye, *Phys. Rev. Lett.* **94**, 173002 (2005).
28. T. Hong, C. Cramer, W. Nagourney, E. N. Fortson, *Phys. Rev. Lett.* **94**, 050801 (2005).
29. Z. W. Barber *et al.*, *Phys. Rev. Lett.* **96**, 083002 (2006).
30. The magnetic field–induced frequency uncertainty is determined from the product of the measured residual magnetic field by means of the clock transition linewidth and experimentally determined frequency shifts versus given magnetic fields along three orthogonal directions. The total systematic uncertainty includes Stark shifts associated with the lattice and the probe beams, magnetic shift, density shift, and blackbody shift. For further details, see M. M. Boyd *et al.*; preprint available at http://arxiv.org/PS_cache/physics/pdf/0611/0611067.pdf.
31. T. P. Heavner, S. R. Jefferts, E. A. Donley, J. H. Shirley, T. E. Parker, *Metrologia* **42**, 411 (2005).
32. S. Bize *et al.*, *J. Phys. B Atom. Mol. Opt. Phys.* **38**, S449 (2005).
33. J. Ye *et al.*, *J. Opt. Soc. Am. B* **20**, 1459 (2003).
34. A. D. Ludlow *et al.*; preprint available at http://arvix.org/ftp/physics/papers/0610/0610274.pdf.
35. A. Brusch, R. Le Targat, X. Baillard, M. Fouche, P. Lemonde, *Phys. Rev. Lett.* **96**, 103003 (2006).
36. H. J. Kluge, H. Sauter, *Z. Phys.* **270**, 295 (1974).
37. A. Lurio, M. Mandel, R. Novick, *Phys. Rev.* **126**, 1758 (1962).
38. L. Olschewski, *Z. Phys. A* **249**, 205 (1972).
39. S. G. Porsev, A. Derevianko, *Phys. Rev. A* **69**, 042506 (2004).
40. R. Santra, K. V. Christ, C. H. Greene, *Phys. Rev. A* **69**, 042510 (2004).

41. We thank T. Parker and S. Diddams for providing the NIST hydrogen maser signal; J. C. Bergquist, I. H. Deutsch, C. H. Greene, J. L. Hall, and P. Julienne for helpful discussions; and X. Huang for technical assistance. The work at JILA is supported by the Office of Naval Research, NIST, and NSF. A.D.L. is supported by NSF–Interdisciplinary Graduate Education, Research and Training and the University of Colorado Optical Science and Engineering Program. T.Z. is a National Research Council postdoctoral fellow. T.I. acknowledges support from the Japan Science and Technology Agency.

10 August 2006; accepted 18 October 2006
10.1126/science.1133732

Macroscopic Hierarchical Surface Patterning of Porphyrin Trimers via Self-Assembly and Dewetting

Richard van Hameren,[1] Peter Schön,[1] Arend M. van Buul,[1] Johan Hoogboom,[2] Sergiy V. Lazarenko,[1] Jan W. Gerritsen,[1] Hans Engelkamp,[1] Peter C. M. Christianen,[1] Hans A. Heus,[1] Jan C. Maan,[1] Theo Rasing,[1] Sylvia Speller,[1] Alan E. Rowan,[1] Johannes A. A. W. Elemans,[1]* Roeland J. M. Nolte[1]

The use of bottom-up approaches to construct patterned surfaces for technological applications is appealing, but to date is applicable to only relatively small areas (~10 square micrometers). We constructed highly periodic patterns at macroscopic length scales, in the range of square millimeters, by combining self-assembly of disk-like porphyrin dyes with physical dewetting phenomena. The patterns consisted of equidistant 5-nanometer-wide lines spaced 0.5 to 1 micrometers apart, forming single porphyrin stacks containing millions of molecules, and were formed spontaneously upon drop-casting a solution of the molecules onto a mica surface. On glass, thicker lines are formed, which can be used to align liquid crystals in large domains of square millimeter size.

The formation of complex submicrometer patterns on surfaces that extend over macroscopic distances underlies the fabrication of integrated circuits and microelectromechanical devices (*1*–*3*). However, for many applications, such as detection arrays and optical elements, well-defined symmetrical patterns can be exploited, especially if the methods decrease the number of processing steps needed or avoid surface-invasive steps that scratch, rub, or etch the surface. Examples of complex pattern formation by noninvasive techniques are still few, usually require large polymeric molecules, and are often of small spatial extent (*4*–*12*). Self-assembly of molecules on a surface can be a simple, versatile, and less time-consuming approach and may lead to defect-free structures (*1*), especially if combined with physical processes such as dewetting and contact-line pinning. Here we report the spontaneous formation of periodic patterns of exceptionally long (up to 1 mm) columnar stacks of porphyrin dye molecules at a solid/liquid interface, with highly defined spatial and parallel ordering. These self-assembled patterns were then used to align liquid crystals (LCs) in domains measuring several square millimeters.

Porphyrin dye molecules can self-organize on a surface into small columnar stacks of submicrometer length (*13*, *14*). These architectures are generated as a result of combined self-assembly and dewetting, which take place simultaneously when a drop-casted solution of the porphyrin molecules is evaporated on a surface. In order to enhance the columnar stacking and hence the length of the assemblies, we have synthesized compound **1** (Fig. 1) (*15*), which consists of three porphyrin moieties that are linked via amide bonds to a central benzene core, a motif that is known to form extended hydrogen-bonded networks (*16*–*19*). Each porphyrin was equipped with three aliphatic hydrocarbon chains to increase the solubility of the stack in organic solvents.

The high tendency of **1** to form aggregates can be directly observed, in that at a concentration of 8 mg/ml, the chloroform solution formed a gel. This strong aggregation is highly dependent on the presence of the alkyl chains, because porphyrin trimers without these chains appeared not to gelate the solvent. In the proton nuclear magnetic resonance (NMR) spectrum of

[1]Institute for Molecules and Materials, Radboud University Nijmegen, Toernooiveld 1, 6525 ED, Nijmegen, Netherlands. [2]Department of Chemistry, Massachusetts Institute of Technology, 77 Massachusetts Avenue, Cambridge, MA 02139, USA.

*To whom correspondence should be addressed. E-mail: j.elemans@science.ru.nl

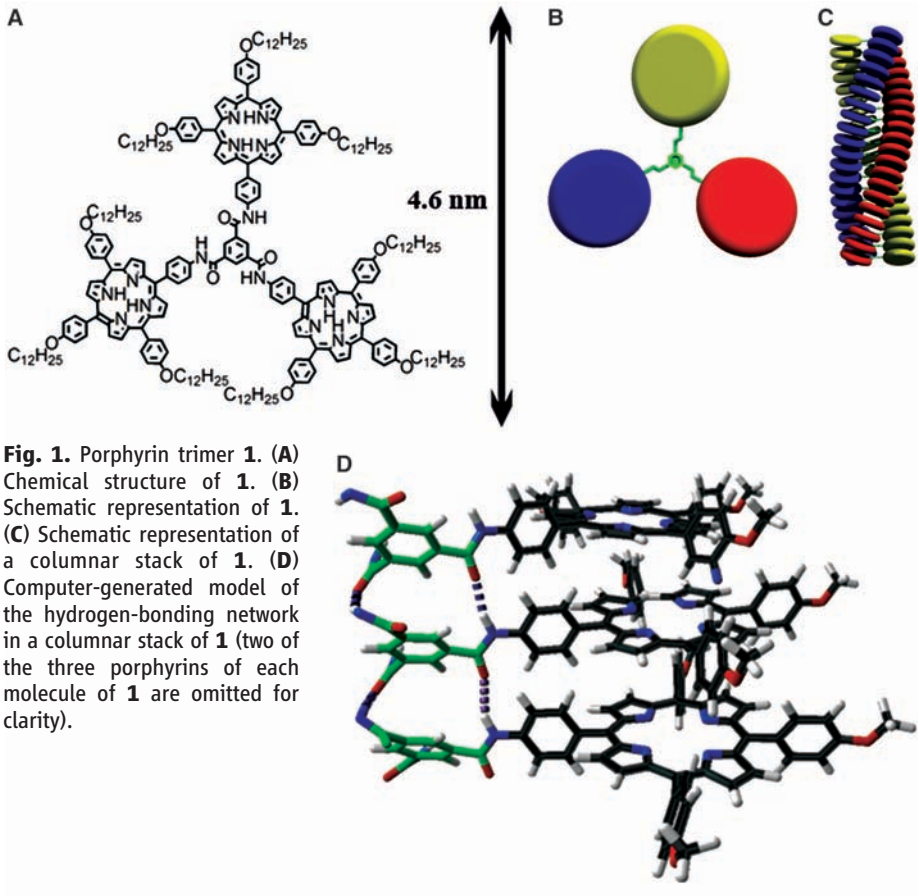

Fig. 1. Porphyrin trimer **1**. (**A**) Chemical structure of **1**. (**B**) Schematic representation of **1**. (**C**) Schematic representation of a columnar stack of **1**. (**D**) Computer-generated model of the hydrogen-bonding network in a columnar stack of **1** (two of the three porphyrins of each molecule of **1** are omitted for clarity).

1 in $CDCl_3$ ([**1**] = 10^{-4} M), very broad peaks were observed, suggesting large aggregate formation. The addition of d^6–dimethyl sulfoxide to this solution caused a sharpening of the NMR signals, which is the result of the solvent breaking up the hydrogen-bonding network (Fig. 1D) and dissolving the aggregates that are present in chloroform.

At the solid/liquid interface, the expected columnar stacking of **1** was confirmed by means of scanning tunneling microscopy (STM) (fig. S1). The aggregation behavior at a surface was further studied with atomic force microscopy (AFM). We drop-casted a diluted solution of **1** in chloroform ([**1**] = 4.8×10^{-6} M, 3-μl droplets) on mica. After evaporation, very large domains (up to ~3 mm^2) containing a highly ordered pattern of equidistant, nearly parallel, wire-like architectures were observed (Fig. 2, A and B). The height of the lines was 4.5 ± 0.4 nm (Fig. 2C), which corresponds remarkably well to the calculated diameter of **1**, indicating a pronounced shape persistence of the molecule. These observations indicate that the lines consisted of a columnar stack one molecule thick, with each of the lines containing millions of molecules. We will argue below that this self-organization of molecules on a macroscopic scale results from a hierarchical dewetting process.

Analysis of several samples revealed a narrow spatial distribution of the periodicity within one single domain [for example, 650 ± 40 nm in a domain with a size of 3 mm^2 (Fig. 2D)], but between several domains the value of the periodicity varied from 0.5 to 1 μm. The lines were oriented parallel with respect to the local solvent front, which can be deduced from the broader contact pinning lines on the sample (Fig. 2E). In addition, at the boundaries of these ordered domains, patterns more reminiscent of normal spinodal dewetting were observed (Fig. 2F). A clear correlation is seen between these two regions, because most columns in the periodic domain appear to grow out from the spinodal dewetting domain.

When larger droplets ([**1**] = 4.8×10^{-6} M, 10 μl in size) were deposited under similar conditions, the longer evaporation time formed porphyrin lines with different dimensions and orientations from those described above (Fig. 3A). A periodicity of 13.4 ± 0.7 μm and a line height of 55.4 ± 0.6 nm were observed. The latter value indicates that each line in this pattern consisted of a bundle of columnar stacks of **1**. Because of the larger dimensions, this pattern could be visualized via optical microscopy (Fig. 3B), which clearly demonstrated that the orientation of the lines, which were up to 0.8 mm long (fig. S3), was now orthogonal with respect to the solvent front. Scanning confocal fluorescence microscopy studies [Fig. 3C, excitation wavelength λ = 411 nm] confirmed that the lines consisted of molecules of **1**, and an emission spectrum characteristic of a porphyrin aggregate (*13*) was obtained (inset, Fig. 3C).

Because mica is birefringent, we could not study the assembly processes optically in real time. We could, however, visualize the line-formation process in real time on a glass surface ([**1**] = 4.8×10^{-5} M, 10-μl droplets), using an optical polarization microscope equipped with a charge-coupled device camera (movie S1). During the evaporation process, the front of the droplet was pinned several times, and upon its withdrawal, deposited material was observed (Fig. 3D). Simultaneously with the pinning, the formation of linear aggregates as a result of the self-assembly processes was already visible within the droplet, perpendicular to the front, before its withdrawal (fig. S2 and movie S1). However, the greater roughness of the glass substrate as compared to mica caused the pattern to be less well-defined.

The formation of the highly ordered line patterns is governed by a combination of molecular self-assembly and other physical processes (*13*). The strong self-assembly of **1**, which is governed by a balanced combination of hydrogen bonding and π–π stacking interactions, is essential for the growth of columnar stacks of almost millimeter length. No members of a wide family of porphyrin macrocycles (hexamers, dodecamers, and porphyrin trimers with ester instead of amide linkers) were able to form similar periodic patterns (*13*). The two primary physical processes that play a major role in pattern formation are contact-line pinning between the edge of a droplet and the surface (the so-called coffee-stain mechanism) and spinodal dewetting (*9*, *20*–*24*). The latter effect is observed when the surface of a thin film on a flat substrate (such as mica) is unstable and deforms spontaneously. Surfaces subject to this kind of dewetting are known to dewet via the formation of an undulating bicontinuous pattern (*24*). We postulate that this undulating pattern governs the spatial distribution of the linear aggregates (Fig. 3E). The small defects observed in Fig. 2A support this postulation, because their presence does not interrupt the periodicity of the patterns.

The initial physical phenomena, contact-line pinning and solvent evaporation, caused the molecules dissolved in the droplet to flow toward the contact line (*9*). In the case of the small droplets (3 μl), the contact line was pinned several times, leaving behind thin layers of deposited molecules of **1** at these positions (Fig. 2, E and G) (*9*). After repeated retractions of the solvent front, thin films remained between the pinned contact lines, which were then subject to spinodal dewetting. Combined with the propensity of **1** to form one-dimensional (1D) aggregates, this dewetting gave rise to the formation of the highly defined periodic patterns, with the contact pinning lines directing their orientation (Fig. 2G). Within each domain, the local spinodal

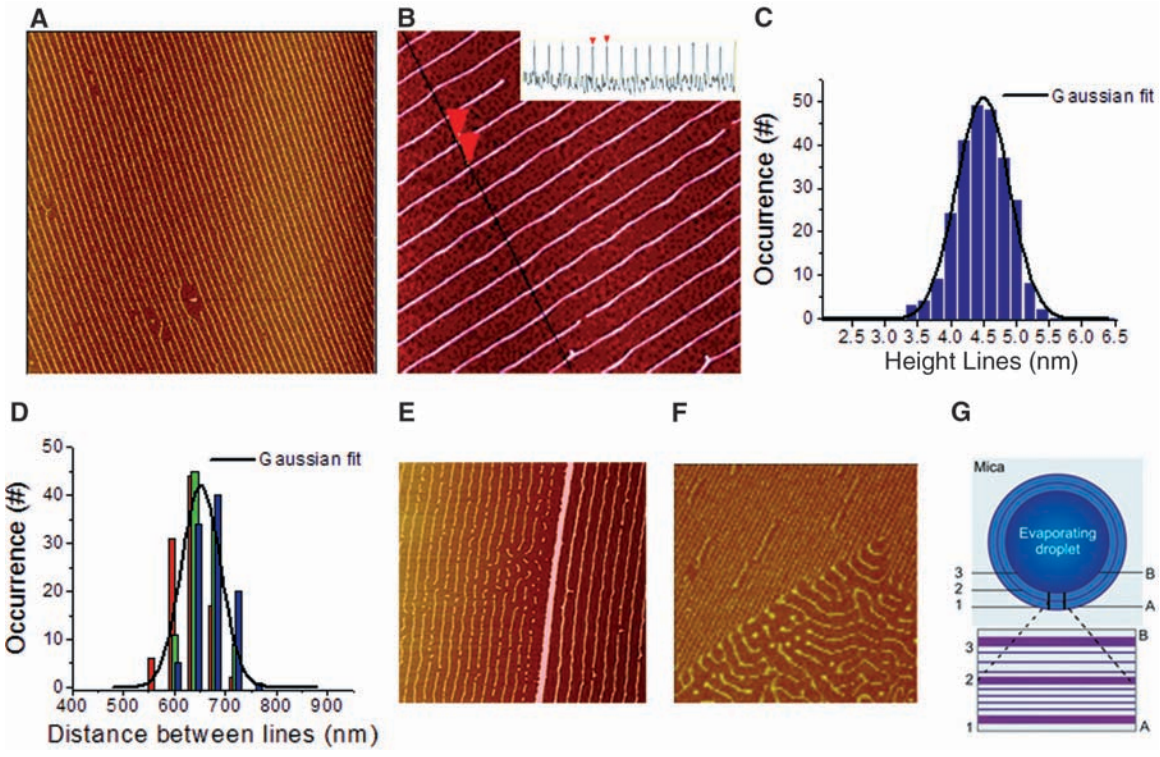

Fig. 2. Patterns formed on mica after the evaporation of 3-μl droplets of compound **1** in chloroform. (**A**) AFM image (scan size = 25 × 25 μm^2) of a pattern of highly ordered equidistant parallel lines. (**B**) AFM image (scan size = 10 × 10 μm^2), with the inset showing the cross section indicated in the AFM image. (**C**) Bar diagram showing the height distribution of the line pattern within a single domain, with the Gaussian fit demonstrating a line height of 4.5 nm, with standard deviation (σ) = 0.4 nm. (**D**) Bar diagram showing the spatial distribution of lines in a single domain (size = 3 mm^2). Each color represents a different position in a single domain. The Gaussian fit demonstrates that within this complete domain, the lines are 650 nm apart and σ = 40 nm. (**E**) AFM image (scan size = 14 × 14 μm^2) showing that the periodic pattern is parallel to the (bold) contact pinning line. (**F**) AFM image (scan size = 40 × 40 μm^2) of a domain transition between a highly ordered and a less ordered domain. (**G**) Mechanism of the formation of the patterned lines. During the evaporation of the droplet (A→B), the contact line is pinned several times, resulting in the formation of contact pinning lines (designated with 1, 2, and 3). After retraction of the solvent front, a thin film remains in which a pattern of thin lines is formed as a result of self-assembly and dewetting.

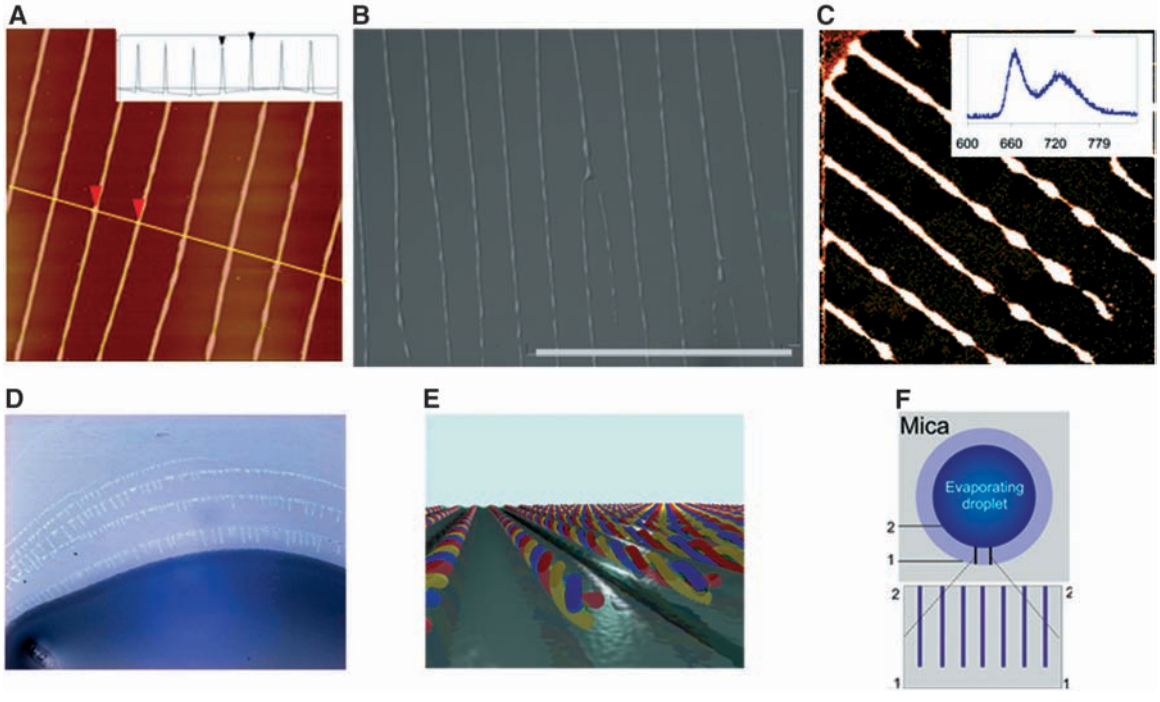

Fig. 3. Patterns formed after the evaporation of 10-μl droplets of compound **1** in chloroform. (**A**) AFM image (scan size = 95 × 95 μm^2) of a line pattern on mica. (**B**) Optical micrograph of the pattern formed on mica (scale bar, 100 μm). (**C**) Scanning confocal fluorescence microscopy image of the lines; the inset shows the characteristic fluorescence spectrum of a porphyrin aggregate, $\lambda_{max\ 1}$ = 665 nm and $\lambda_{max\ 2}$ = 726 nm. (**D**) Optical micrograph of the coffee-stain–like pattern formed during the evaporation of a solution of **1** in chloroform on glass ([**1**] = 4.8 × 10^{-5} M); the bottom part is still covered with solution (dark blue). The whitish stripes are the aggregates that remain after retraction of the droplet. (**E**) Proposed formation of periodic patterns on flat mica; spinodal dewetting causes an undulating pattern in the solvent, which governs the positioning of the aggregates and thus the spatial distribution of the lines. (**F**) Mechanism of the formation of the patterned lines. The presence of aggregates preformed in solution hinders the retraction of the solvent front from 1 to 2, causing partial pinning of the contact line. In combination with the molecular self-assembly, this partial pinning results in an orientation and growth of linear aggregates orthogonal to the local solvent front; contact pinning lines are not observed.

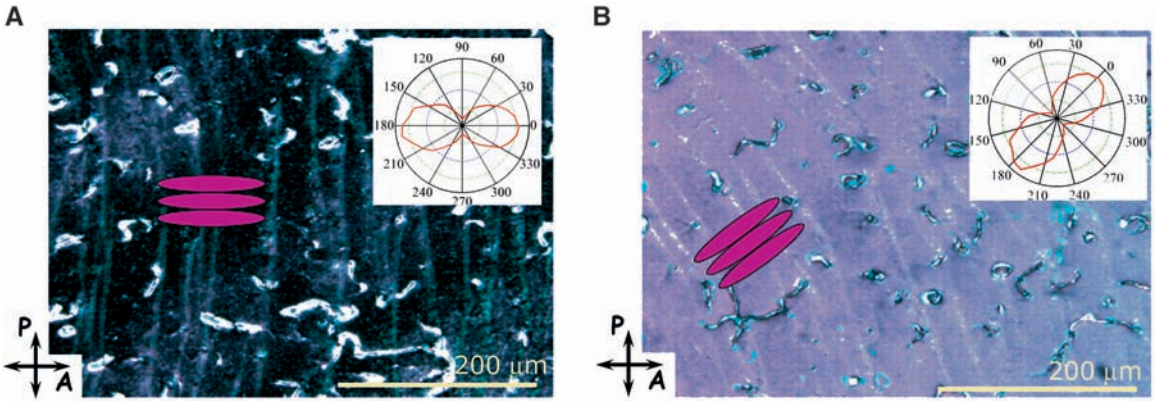

Fig. 4. Application of the patterns formed by **1** on a glass substrate as alignment layers for 5CB; polarizing microscopy images of a LC cell between crossed polarizers (denoted by P and A). (**A**) LC ordering parallel to the analyzer. (**B**) Texture after rotation of the sample over 45°. The local orientation of the 5CB molecules, deduced from the SHG rotational anisotropy patterns (insets), is depicted schematically in both images.

dewetting determined the periodicity, which in all cases was between 500 nm and 1 μm.

In the case of the larger droplets (10 μl), the evaporation of the solvent took longer and allowed the formation of larger aggregates already in solution, which were subsequently deposited (Fig. 3, A and B). Apparently, there was not enough material present at the contact line to completely pin it (*9*). The resulting partial pinning of the solvent front hindered the retraction of the contact line, and in contrast to the experiments with the smaller droplets, contact pinning lines were then not formed (Fig. 3F) (*9*). The partial pinning caused a flow of molecules toward and orthogonal to the contact line. The concomitant local increase in the concentration of molecules of **1** led to growth of the lines from a direction opposite to the molecular flow, resulting in an orthogonal orientation with respect to the solvent front. The combination of (i) the tendency of the molecules to form 1D aggregates, (ii) the occurrence or absence of contact line pinning, and (iii) spinodal dewetting effects resulted in the observed surface patterning in the two cases.

Previous reports have described organized assemblies of polymers (*25*), dendrimers (*3*, *26*, *27*), and block copolymers (*28*), leading to crystal-like domains on surfaces. In none of these cases, however, have 1D single molecular stacks spontaneously organized into periodic dissipative patterns been observed. Unlike our experiments, constructing such patterns requires invasive techniques such as lithography or sliding glass plates (*29*, *30*).

The line patterns obtained with the large droplets were investigated as possible LC alignment layers. LC cells, consisting of one glass plate covered with the aggregates and a non-rubbed counter-plate spin-coated with a commercially available polyimide, were prepared and filled with 4-cyano-4′-pentyl biphenyl (5CB) molecules in the isotropic phase to avoid flow alignment. Polarizing microscopy showed that the cells contained aligned LC domains of several square millimeters (Fig. 4) in the regions of the linear aggregates and no alignment in other areas. Closer inspection showed that the alignment was interrupted by concentric circles, which were the contact pinning lines (Fig. 3D).

The contact pinning lines themselves do not align the LC molecules but remain visible, which indicates that the formed aggregates are the ones that act as a command layer. Second harmonic generation (SHG) measurements confirmed that the mesogenic molecules were uniformly aligned parallel to the radially oriented stacks of **1** [that is, perpendicular to the contact lines, in exceptionally large domains (1 cm^2) (Fig. 4)]. As for most anisotropic surfaces that show LC alignment (*31*), the alignment was probably due to (i) a minimization of elastic energy and (ii) the presence of molecular interactions between the LC molecules and the oriented columnar stacks (*32*). In the case of the ordered porphyrin patterns, however, dipole-dipole interactions in particular are expected to have a large effect, because the head-to-tail orientation of the amide functions within the linear aggregates, as shown in Fig. 1D, creates a macroscopic dipole moment parallel to the stacking axis (*17*). The use of periodic patterns created by controlled self-organization may lead to a viable and cheap alternative to current methods of forming alignment layers.

The remaining challenge in exploiting this phenomenon will now be to further control the self-assembly in such a way that surface patterns can be oriented at will. Control over the periodic arrays might be accomplished by patterned heating of the surface with the use of laser gratings or by application of an electric field to align the high intrinsic dipole moments of the stacks. Extra stabilization of the patterns can be achieved by introducing cross-linkable groups (such as cinnamate, thiophene, or methacrylate units) in the alkyl chains, which would allow modification of the patterns after their deposition on the surface. The self-assembly/dewetting technique could also be applied in conjunction with conventional (photo-)lithographic or stamping methods.

References and Notes

1. H. O. Jacobs, A. R. Tao, A. Schwartz, D. H. Gracias, G. M. Whitesides, *Science* **296**, 323 (2002).
2. T. Verbiest *et al.*, *Science* **282**, 913 (1998).
3. V. Percec *et al.*, *Nature* **419**, 384 (2002).
4. R. D. Deegan *et al.*, *Nature* **389**, 827 (1997).
5. M. A. Ray, H. Kim, L. Jia, *Langmuir* **21**, 4786 (2005).
6. K. Mougin, H. Haidara, *Langmuir* **18**, 9566 (2002).
7. J. V. Barth *et al.*, *Angew. Chem. Int. Ed.* **39**, 1230 (2000).
8. M. A. Ray, H. Kim, L. Jia, *Langmuir* **21**, 4786 (2005).
9. R. D. Deegan, *Phys. Rev. E Stat. Phys. Plasmas Fluids Relat. Interdiscip. Topics* **61**, 475 (2000).
10. J. Huang, F. Kim, A. R. Tao, S. Conner, P. Yang, *Nat. Mater.* **4**, 896 (2005).
11. S. Vyawahare, K. M. Craig, A. Scherer, *Nano Lett.* **6**, 271 (2006).
12. I. I. Smalyukh *et al.*, *Phys. Rev. Lett.* **96**, 177801 (2006).
13. M. C. Lensen *et al.*, *Chem. Eur. J.* **10**, 831 (2004).
14. C. R. L. P. N. Jeukens *et al.*, *Nano Lett.* **4**, 1401 (2004).
15. Materials and methods are available as supporting material on *Science* Online.
16. S. Ranganathan *et al.*, *Chem. Commun.* **2001**, 2544 (2001).
17. M. L. Bushey, T. Q. Nguyen, W. Zhang, D. Horoszewski, C. Nuckolls, *Angew. Chem. Int. Ed.* **43**, 5446 (2004).
18. A. J. Wilson, M. Musada, R. P. Sijbesma, E. W. Meijer, *Angew. Chem. Int. Ed.* **44**, 2275 (2005).
19. M. P. Lightfoot, F. S. Mair, R. G. Pritchard, J. E. Warren, *Chem. Commun.* **1999**, 1945 (1999).
20. A. Sharma, R. Khanna, *Phys. Rev. Lett.* **81**, 3463 (1998).
21. A. Sharma, R. Khanna, *J. Chem. Phys.* **110**, 4929 (1999).
22. G. Reiter, *Science* **282**, 888 (1998).
23. A. M. Higgins, R. A. L. Jones, *Nature* **404**, 476 (2000).
24. A. Sharma, J. Mittal, R. Verma, *Langmuir* **18**, 10213 (2002).
25. M. H. Stenzel, C. Barner-Kowollik, T. P. Davis, *J. Polym. Sci. Part Polym. Chem.* **44**, 2363 (2006).
26. S. D. Hudson *et al.*, *Science* **278**, 449 (1997).
27. V. Percec *et al.*, *Nature* **430**, 764 (2004).
28. S. I. Stupp *et al.*, *Science* **276**, 384 (1997).
29. H. Yabu, M. Shimomura, *Adv. Funct. Mater.* **15**, 575 (2005).
30. Z. Lin, S. Granick, *J. Am. Chem. Soc.* **127**, 2816 (2005).
31. M. Behdani *et al.*, *Appl. Phys. Lett.* **80**, 4635 (2002).
32. T. Rasing, I. Musevic, *Surfaces and Interfaces of Liquid Crystals* (Springer, Heidelberg, 2004).
33. Supported by grants from the Netherlands Organization of Scientific Research (NWO) to R.J.M.N. (TOP grant), to J.A.A.W.E. (VENI grant), to P.S. (FOM/ALW), and to A.E.R. (VIDI grant); the National Research School Combination Catalysis (NRSC-C) to R. van H. and to R.J.M.N.; and the Royal Netherlands Academy of Science to R.J.M.N.

Supporting Online Material

www.sciencemag.org/cgi/content/full/314/5804/1433/DC1
Materials and Methods
Figs. S1 to S4
Reference
Movie S1

25 July 2006; accepted 28 September 2006
10.1126/science.1133004